



## S,N-doped carbon dots as a fluorescent probe for bilirubin

R. R. Anjana<sup>1</sup> · J. S. Anjali Devi<sup>1</sup> · M. Jayasree<sup>1</sup> · R. S. Aparna<sup>1</sup> · B. Aswathy<sup>1</sup> · G. L. Praveen<sup>1</sup> · G. M. Lekha<sup>1</sup> · George Sony<sup>1</sup>

Received: 13 October 2017 / Accepted: 9 November 2017 / Published online: 5 December 2017  
© Springer-Verlag GmbH Austria, part of Springer Nature 2017

### Abstract

Carbon dots doped with sulfur and nitrogen (S,N-CDs) were utilised to design a paper-stripe based fluorescent probe for the detection of bilirubin. The S,N-CDs were synthesized through a microwave assisted route by using citric acid as carbon source and L-cysteine as a source of nitrogen and sulfur. The S,N-CDs exhibit bright blue fluorescence emission with a peak at 452 nm. Fluorescence is quenched by Fe(III) but selectively restored by bilirubin. The quenched fluorescent probe exhibit significant selectivity and sensitivity for bilirubin in the 0.2 nM to 2 nM concentration range, with a 0.12 nM detection limit. The method was applied to the determination of bilirubin in spiked human serum and urine samples. The method was used to design a paper based test stripe as a point of care device for visual bilirubin detection.

**Keywords** Fluorescence assay · Hyperbilirubinemia · Paper based test stripe · Quenching · Aggregation · Static quenching · Inner filter effect · Electron transfer · Fluorescence turn on · Jaundice

### Introduction

Neonatal jaundice is recognized as one of the major healthcare issues facing by developing countries [1]. The accumulation of bilirubin (BR) in blood develops a condition called hyperbilirubinemia, when BR in blood plasma crosses  $19.80 \text{ mg}\cdot\text{mL}^{-1}$  in newborn and  $1.19 \times 10^{-2} \text{ mg}\cdot\text{mL}^{-1}$  in adults [2]. BR is generated in human body as a result of heme catabolism and is excreted via bile. Yellow coloration of skin and sclera in association with jaundice is the symptom of elevated level of BR accumulation [3]. Toxic level of BR result in neurotoxicity in newborns which leads to neurodevelopmental abnormalities such as hearing loss, athetosis, rarely intellectual

deficits and even extreme condition results in mortality or life-long neurologic sequelae (kernicterus) [1]. Early diagnosis and treatment of hyperbilirubinemia is the only way to overcome this critical situation.

Available analytical methods to detect BR in serum sample are diazo methods, peroxidase methods, separation based methods and fluorometric methods [4]. Among these, fluorometric methods are simple, fast and easy. Fluorescent nanoprobe of metal nanoclusters, quantum dots and carbon dots (CDs) are currently employed for detecting various biomolecules [5, 6]. However, requirements of expensive precursors for metal nanoclusters and toxicity of quantum dots restricts its translation from bench side to bed side.

CDs are quasi-spherical nanoparticles with diameter less than 10 nm [7]. CDs received much attraction due to its cost-effective preparation, biocompatibility, low toxicity and optical properties [7]. They have potential applications in chemical sensing, nanomedicine, photo catalysis, electro catalysis, bioimaging and biosensing [7]. CDs can be synthesized through arc-discharge, laser ablation, electrochemical synthesis, thermal combustion, hydrothermal, template and microwave (MW) method [7]. Among these, MW method is fast and inexpensive method to synthesize CDs with good optical properties [7]. Heteroatom doping of CDs by

**Electronic supplementary material** The online version of this article (<https://doi.org/10.1007/s00604-017-2574-8>) contains supplementary material, which is available to authorized users.

✉ George Sony  
emailtosony@gmail.com

<sup>1</sup> Department of Chemistry, School of Physical and Mathematical Sciences, University of Kerala, Kariavattom Campus, Thiruvananthapuram, Kerala 695581, India

Nitrogen, Sulfur, Boron and Phosphorous improves quantum yield by the creation of various surface functionalities and surface defects which favor fluorescence. Various methods to synthesize carbon dot that have been reported in the literature are correlated in Table S1.

CDs based fluorescence turn off detection of various metal ions like Hg(II), Fe(III), Co(II), Cr(VI) [8, 9], biomolecules like glucose [10] heparin [11] and reactive oxygen species like H<sub>2</sub>O<sub>2</sub> [12] are reported in literature. Moreover, sensing mode of ON-OFF-ON for the detection of ascorbic acid, 4-nitrophenol, quercetin, 2, 4-dinitrophenol based on CDs have been explored [8, 13, 14]. Turn on detection is more effective compared to turn off detection as it is easy to detect a bright signal in dark background rather than a bright signal in a bright background [15].

In the present work, sulfur and nitrogen doped carbon dots (S,N-CDs) were prepared from citric acid (CA) and L-Cysteine. CA is an adaptable starting material for the synthesis of CDs by bottom-up routes due to various surface functionalities like -COOH, -OH and act as a carbon precursor [16–18]. L-Cysteine, a proteinogenic amino acid act as nitrogen and sulfur source [19]. Furthermore, it has antioxidant, anti-inflammatory properties and has the ability to neutralize heavy metals present in the body [19]. The fluorescent intensity of S,N-CDs can be significantly quenched by Fe(III) ions [20] and can be effectively restored by the addition of BR due to its tetrapyrrole ring structure which has an affinity towards Fe(III). It has been reported that Cu(II) quenched gold nanoclusters were employed for the detection of BR [2]. In this background, we tried to develop a CDs based low cost fluorescence turn on assay for BR. Turn on fluorescence analysis were performed in BR spiked human serum and urine samples. Practical applicability was further envisaged by designing paper based test stripe for direct detection of BR.

## Experimental

### Materials

L-Cysteine, Bilirubin and Hemoglobin were purchased from TCI, Tokyo, Japan ([www.tcichemicals.com](http://www.tcichemicals.com)). Citric acid anhydrous Pure, Ferric chloride hexahydrate, Potassium chloride, Cholesterol extra pure, Ammonium Ferric Sulphate decahydrate, Silver Nitrate, Zinc Chloride dry Purified and Ferrous Chloride tetrahydrate for analysis were brought from Merck Specialities Pvt. Ltd., Mumbai ([www.merck.co.in](http://www.merck.co.in)). Quinine Sulphate and Glutathione ( $\geq 98.0\%$ ) were purchased from Sigma Aldrich ([www.sigmaldrich.com](http://www.sigmaldrich.com)). Cobalt Sulphate and Cadmium acetate were brought from Sisco Research Laboratories Pvt. Ltd. ([www.srlchem.com](http://www.srlchem.com)). Ferric acetate and Manganese Chloride (97.0%) from Otto chemie Pvt. Ltd. ([www.ottokemi.com](http://www.ottokemi.com)). Copper Sulphate,

Sodium Chloride, Calcium Nitrate, Magnesium sulphate, Urea, Acetone and Mercuric Chloride (98.0%) were brought from NICE chemicals Pvt. Ltd., Kochi ([www.nicechemicals.com](http://www.nicechemicals.com)). Nickel Chloride hexahydrate Pure, D (-)-Fructose, D-Galactose extrapure, D-Glucose anhydrous were purchased from SRL Pvt. Ltd., Mumbai ([www.srlchem.com](http://www.srlchem.com)). Sodium Hydroxide, Creatine and Uric Acid Stock Standard Solution (0.1%) were brought from Spectrum chemicals, India ([www.spectrumchemical.com](http://www.spectrumchemical.com)).

### Instruments

The room temperature fluorescence measurements of all samples were studied using Jasco FP-750 spectrofluorometer. High Resolution TEM images of S,N-CDs were taken in a JEOL JEM 2100 multipurpose, 200 kv analytical electron microscope. DLS measurements were carried out in HORIBA Scientific nano partica nanoparticles analyser SZ-100. The samples were analyzed in UV-Visible spectroscopic study using Perkin Elmer Lambda 365 UV Visible spectrophotometer. The functional group analysis is carried out using ATR-FTIR is performed using Agilent technologies Cary 630 FTIR spectrometer. Digital pH meter MK VI of systronics was used to measure the pH. The samples were prepared by microwave irradiation using POWER SOLO 17D, ONIDA instrument. Fluorescence lifetimes of all samples were carried out in Fluorolog Fluorescence Spectrophotometer, Horiba, USA using time-correlated single photon counting (TCSPC).

### Synthesis of fluorescent S,N-CDs

CDs were synthesized via microwave irradiation method [21]. Citric acid anhydrous (0.2 g) was mixed with L-cysteine (0.4 g) in 4.0 mL water. Then, it was irradiated at 700 W for 40 s in a microwave oven. A thick syrupy colorless liquid obtained was diluted to 3.0 mL and the concentration becomes 3.902  $\mu\text{g}\cdot\text{mL}^{-1}$ . A dialysis membrane (MWCO: 1KDa); was then used to separate the S,N-CDs from any residual unreacted species.

### Fe(III) modulated S,N-CDs

The stock solutions of Na(I), K(I), Mg(II), Ca(II), Cr(III), Mn(II), Fe(III), Fe(II), Co(II), Ni(II), Cu(II), Ag(I), Zn(II), Cd(II) and Hg(II) were prepared with 50 mM concentrations. In a typical assay, 20  $\mu\text{L}$  of metal ion solution was mixed with 3.0 mL of S,N-CDs at pH 2.5 in room temperature before spectral measurements. The sensitivity was confirmed by adding serial concentrations of Fe(III) and all other metal ions in a similar way. The PL spectra were obtained at an excitation wavelength of 375 nm.

## Detection of bilirubin

The stock solutions of bilirubin were prepared by taking 0.146 g bilirubin, add 20  $\mu\text{L}$  1 M NaOH to dissolve and made up to 15 mL by adding distilled water. S,N-CDs was semi quenched with Fe(III) [0.98 mM]. The sensitivity was studied by adding 20  $\mu\text{L}$  of 3.80 nM of bilirubin in a sequential manner. All biomolecules (glucose, fructose, glutathione, galactose, cholesterol, urea, uric acid, creatine, hemoglobin) and bilirubin were studied in the same manner.

## Real sample assay

Serum samples were collected from healthy volunteers in morning without EDTA stabilization as it may interfere with the turn on response of bilirubin towards Fe(III) quenched S,N-CDs. Then, it was spiked with bilirubin and diluted 10, 100, 1000 times, before analysis. Concentration of bilirubin spiked in 10 times diluted urine sample = 0.27  $\mu\text{M}$  (critical concentration of bilirubin in hyperbilirubinemia condition) which was further diluted to 100 and 1000 times. Concentration of bilirubin spiked in serum sample = 340  $\mu\text{M}$  (elevated concentration of bilirubin in newborn) and 170  $\mu\text{M}$  (elevated concentration of bilirubin in adult) which was again diluted to 10, 100 and 1000 times.

## Paper based test stripe assay

Whatmann No. 40 filter paper was used for the detection of bilirubin with a dimension of  $8 \times 1$  cm. It was soaked with S,N-CDs and then dried. This S,N-CDs impregnated paper stripe was further soaked with different concentration of Fe(III) (1 mM, 5 mM, 10 mM, 15 mM, 20 mM, 25 mM) and again dried. Then, different concentration of bilirubin (0.33  $\mu\text{M}$ , 0.66  $\mu\text{M}$ , 0.99  $\mu\text{M}$ , 1.33  $\mu\text{M}$ , 1.66  $\mu\text{M}$ , 1.99  $\mu\text{M}$ ) was added to the semi quenched system (5 mM of Fe(III)). Fluorescence is visualized under UV illumination of 366 nm.

## Results and discussion

### Synthesis and characterisation of S,N-CDs

S,N-CDs synthesized *via* MW mediated method in contrast to the previously reported hydrothermal technique [21]. Experimental conditions for MW synthesis were optimized to tune the fluorescence of S,N-CDs. Three factors such as molar ratio of the precursors, MW irradiation power and time of irradiation were optimized (Fig. S1-S2). At the optimum conditions (700 W, 40 s) colorless highly viscous liquid was formed due to the simultaneous formation of carbonized nanoparticles and citrazinic acid (molecular fluorophore) derivatives (Fig. S3, S4) [22]. The fluorescent S,N-CDs was again diluted with

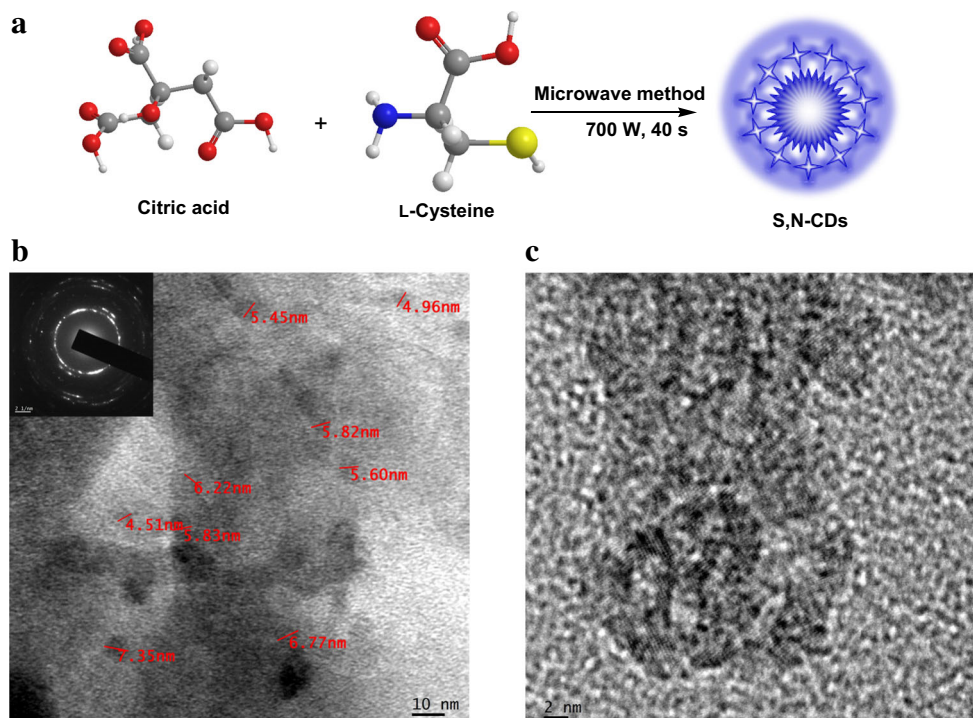
3.0 mL water to perform further characterizations. The resulted fluorophores of citrazinic acid derivatives attached to the surface and interiors of carbon backbone was expected to elicit fluorescence. Maximum fluorescence emission for S,N-CDs was obtained with MW irradiation of 700 W for 40 s at 452 nm. At MW power higher than this, carbonization process predominates over fluorophore formation resulting in a charred mass. The concentration of this optimized S,N-CDs [S,N-CDs] was calculated to be 3.902  $\mu\text{g}\cdot\text{mL}^{-1}$ .

In order to get an idea about morphology and size distribution, High Resolution Transmission Electron Microscopic (HRTEM) characterization was carried out. HRTEM image reveals that the synthesized S,N-CDs are spherical in shape with a size range of  $6 \pm 1.5$  nm (Fig. 1b and c). The Selected Area Electron Diffraction (SAED) pattern (*inset* of Fig. 1b) of S,N-CDs reveals that crystalline entities are embedded in an amorphous matrix. Dynamic Light Scattering (DLS) measurements of S,N-CDs provides a hydrodynamic diameter value of  $47 \pm 7$  nm (Fig. S5) which was significantly larger than values from TEM images indicating the self assembly of citric acid based carbon dots into aggregates in polar solvents like water. The maximum fluorescence emission peak was observed at 452 nm upon the excitation of 375 nm and this wavelength is fixed for further studies (Fig. S6).

UV/Vis absorption spectrum of S,N-CDs shows an absorption peak at 352 nm, which can be assigned to  $n \rightarrow \pi^*$  transition of C=O functionalities present in S,N-CDs (Fig. S7) similar to that of the transitions in citrazinic acid [22]. The UV/Vis absorption band corresponding to the  $\pi \rightarrow \pi^*$  transitions are very weak. S,N-CDs shows bright blue fluorescence under UV illumination of 366 nm. Interestingly, on applying different excitation wavelength from 300 to 425 nm, the emission peak remains constant (Fig. 2a). This excitation independent emission behavior of CDs obey Kasha-Vavilov rule similar to citrazinic acid [23]. Disparity exists in literature regarding obedience and disobedience of Kasha-Vavilov rule in the luminescence of CDs [7, 20, 23, 24]. This elusive nature of S,N-CDs can be accorded by the different precursors and synthetic conditions adopted. The quantum yield of S,N-CDs was obtained as  $78 \pm 10\%$  (Table S2).

ATR-FTIR spectra was used to identify the surface functionalities present on S,N-CDs. In ATR technique the absorption of carbon sample becomes greater with deeper light penetration at longer wavelength. Carbon sample displays absorption over the entire range from 4000 to 400  $\text{cm}^{-1}$ . This causes the observed base line dip towards the right end of the spectrum. The broad band at 3401  $\text{cm}^{-1}$  represents stretching vibration of O-H and N-H respectively. The peak at 2563  $\text{cm}^{-1}$  represents the stretching vibration of S-H [21]. A strong signal at 1702  $\text{cm}^{-1}$  in S,N-CDs is due to the C=O stretching vibration of  $\alpha,\beta$ -unsaturated carboxylic acid moieties, which is present in citrazinic acid and its derivatives [22]. The peak at 1616  $\text{cm}^{-1}$  was attributed to C=C stretching vibrations [21]. The peaks at 1911  $\text{cm}^{-1}$  and

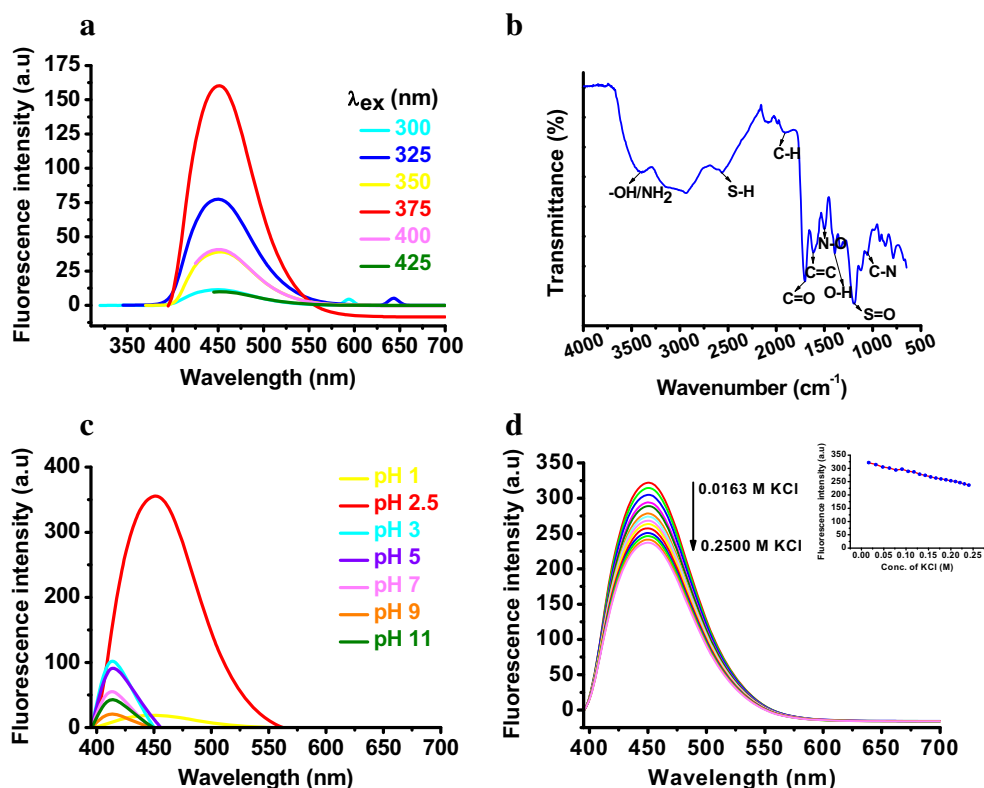
**Fig. 1** **a** Scheme depicting synthesis of S,N-CDs. **b** Transmission Electron Microscopic (TEM) image of synthesized S,N-CDs; (*inset*: SAED pattern of S,N-CDs). **c** High Resolution Transmission Electron Microscopic (HRTEM) image of S,N-CDs



$1393\text{ cm}^{-1}$  are assigned to C-H bending vibration of aromatic compound and O-H bending vibration of phenol [22]. The peak at about  $1054\text{ cm}^{-1}$  is due to the stretching vibration of C-N (Fig. 2b) [21]. These observations attest the existence of citrazinic acid derivatives in carbon dot framework.

The mechanism underlying the origin of fluorescence in CDs is still not certain. One of the widely accepted mechanisms is based on quantum confinement effect of CDs [8]. It has also been reported that defective surface states are the dominant factor for controlling fluorescence behavior of CDs compared

**Fig. 2** **a** Fluorescence spectra of S,N-CDs at different excitation wavelengths ranging from 300 to 425 nm, pH -2.5,  $[\text{S,N-CDs}] = 3.902\text{ }\mu\text{g}\cdot\text{mL}^{-1}$ . **b** ATR-FTIR spectrum of S,N-CDs at synthesized, pH -2.5. **c** Fluorescence emission spectra of S,N-CDs at various pH conditions: 1, 2.5, 3, 5, 7, 9, 11. **d** Fluorescence response of S,N-CDs with increasing ionic strength; ( $[\text{KCl}] = 0.0163\text{ M} - 0.25\text{ M}$ ), pH -2.5,  $\lambda_{\text{ex}} = 375\text{ nm}$



to quantum size effect [17, 25]. CDs have high  $sp^2$  character with plenty of isolated  $\pi$  conjugate domains which in turn favors quantum confinement effect and band gap transitions to cause electron-hole pair recombination [8]. The second theory supports the defective state emission associated with surface defects [8]. CDs resemble graphene oxide as it symbolizes graphite nanocrystals with high heteroatom content [26]. The nitrogen linkage, disorder the carbon hexagonal ring and produce emissive energy traps. The sulphur atom also creates emissive energy traps. For sulphur and nitrogen doped carbon dots, the introduction of sulphur atom can enhance the effect of nitrogen atom. [27]. The molecular origin of fluorescence in the citric acid based CDs has also been attributed to the presence of derivatives of citrazinic acid [22]. Citric acid contains three carboxyl functionalities, which undergo intramolecular condensation and cyclisation with  $\beta$ -amino thiols like cysteine to form derivatives of citrazinic acid [22].

For further applications, the influence of pH towards the fluorescence intensity of S,N-CDs was monitored (Fig. 2c). For a wide range of pH values from 1 to 11, the fluorescence intensity of S,N-CDs increases with the decrease of pH and maximum fluorescence was observed at synthesized pH 2.5. The pH dependent fluorescence of S,N-CDs was due to the three possible prototropic equilibria, phenol  $\leftrightarrow$  phenolate,

carboxylic  $\leftrightarrow$  carboxylate and ammonium  $\leftrightarrow$  amine ion that occurs in S,N-CDs [28]. The  $n \rightarrow \pi^*$  transition gains much predominance in polar protic medium where  $\pi \rightarrow \pi^*$  transitions are very weak. The maximum fluorescence was observed at acidic pH due to the much stabilization of  $n \rightarrow \pi^*$  transitions in aqueous polar medium than in non-polar medium. The shelf life of S,N-CDs was monitored by storing it at 4 °C for 37 days and fluorescence intensity is found to remain stable (Fig. S8). The stability in KCl solution was checked and found that the fluorescence intensity of S,N-CDs shows a slight decreasing trend with the increase in ionic strength (Fig. 2d). Increasing ionic strength may cause aggregation of S,N-CDs and restricting its fluorescence. The average fluorescence lifetime of S,N-CDs was obtained as  $7.8 \pm 0.2$  ns (Fig. S9). The fluorescence decay curve of S,N-CDs is fitted in a tri-exponential function consisting of 3.97 ns (4.15%), 7.94 ns (96.83%) and 15.8 ns (-0.98%) contributing components.

### Turn off phenomena in S,N-CDs

The fluorescence response of S,N-CDs with sequential addition of Fe(III) was investigated. As demonstrated in Fig. 3a, upon addition of Fe(III), the blue fluorescence intensity continuously decreased and the emission peak get slightly red

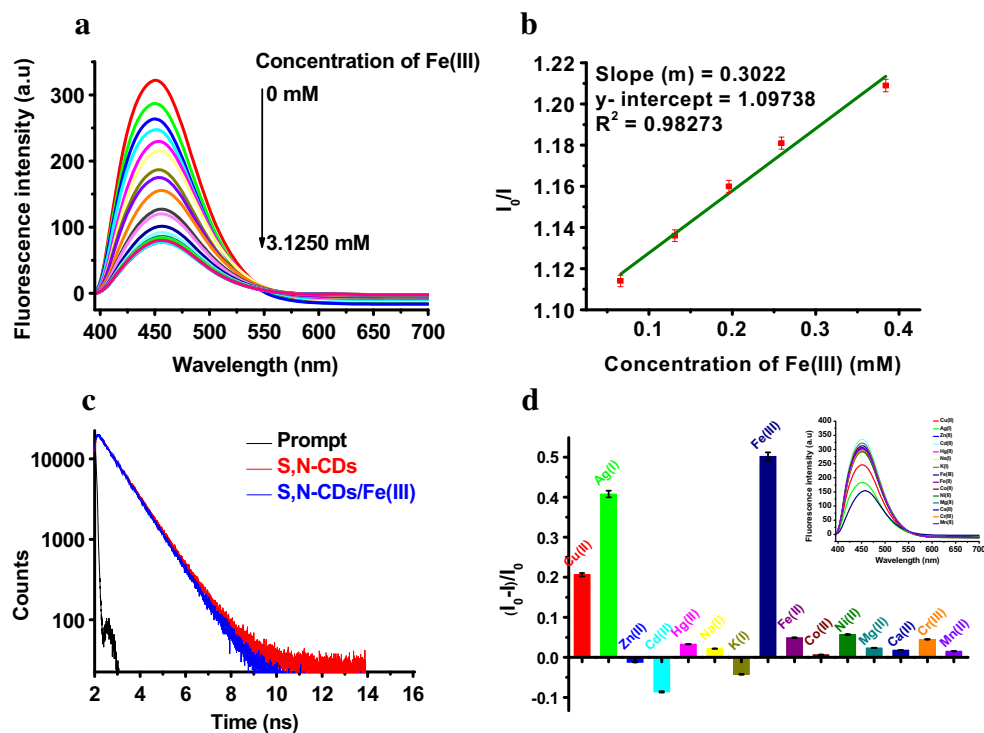


**Fig. 3** **a** Fluorescence response of S,N-CDs upon the addition of various concentrations of Fe(III). ([Fe(III)] = 0 mM - 3.1250 mM), pH -2.5,  $\lambda_{ex}$  = 375 nm. **b** The Stern-Volmer plot revealing linear fluorescence quenching of S,N-CDs by the addition of Fe(III);  $I_0$  is the initial fluorescence intensity of S,N-CDs and  $I$  is the fluorescence intensity after the addition of Fe(III).  $\lambda_{ex}$  = 375 nm; [Fe(III)] = 0.066 mM to 0.384 mM. **c** The time resolved fluorescence decay profile of S,N-CDs (red) and Fe(III)

quenched with bilirubin (blue);  $\lambda_{ex}$  = 330 nm,  $\lambda_{em}$  = 452 nm ([Fe(III)] in quenched S,N-CDs = 1.61 mM). **d** The effect of various metal ions on the fluorescence response of S,N-CDs at pH 2.5;  $I_0$  is the fluorescence intensity of S,N-CDs after the addition of corresponding metal ions. (Inset: the fluorescence spectra showing the effect of different metal ions on S,N-CDs), ([metal ions] = 0.33 mM)

shifted to 457 nm. The Stern-Volmer plot depicting fluorescence quenching effect on S,N-CDs by the addition of Fe(III) from 0.066 mM to 0.384 mM;  $(I_0/I) = 0.3022c + 1.09738$ ; ( $R^2 = 0.98273$ ), where  $c$  is the concentration of Fe(III) (mol/L),  $I_0$  is the fluorescence intensity of S,N-CDs and  $I$  is that of quenched S,N-CDs by the addition of Fe(III) (Fig. 3b). The detection limit of Fe(III) was obtained as 23.08  $\mu$ M (based on  $3\sigma/\text{slope}$ ,  $\sigma$  is the standard deviation) and the quenching efficiency of Fe(III) was found to be 76.22%.

Fe(III) induced fluorescence quenching was monitored over the pH range from 1 to 11. The maximum quenching was obtained at 2.5 (Fig. S10) and this pH was taken for further investigations. In acidic medium, the phenolic groups present in citrazinic acid derivatives have more affinity towards Fe(III). As shown in Fig. 3c, the decay curve of S,N-CDs/Fe(III) shows a tri-exponential pathway consisting of 3.82 ns (4.36%), 7.65 ns (97.06%) and 15.30 ns (-1.42%) similar to that of S,N-CDs. The average fluorescence lifetime of S,N-CDs/Fe(III) was about  $7.6 \pm 0.4$  ns.

Generally, the possible quenching mechanisms manifesting in CDs are static quenching, dynamic quenching, Förster resonance energy transfer (FRET), photo induced electron transfer (PET), inner filter effect (IFE) [29] and aggregation induced quenching [30]. The ratio of average fluorescence lifetime of S,N-CDs ( $\tau_0 = 7.8 \pm 0.2$  ns) to S,N-CDs/Fe(III) ( $\tau = 7.6 \pm 0.4$  ns) was approximately unity ( $\tau_0 / \tau \approx 1$ ) and such consistency in fluorescence lifetime of two systems supports static quenching mechanism. Thus, possibility of dynamic, FRET and PET quenching mechanisms can be sidelined because such quenching mechanisms must be accompanied by significant change in fluorescent lifetime between S,N-CDs and turn off system. Static quenching occurs by the formation of non fluorescent ground-state complex through the interaction between S,N-CDs and Fe(III) [31]. Fe(III) absorbs and reacts with phenolic -OH, -COOH and -NH<sub>2</sub> groups present on the surface of S,N-CDs leading to chelation or co-ordination. These complexations facilitate non-radiative electron-hole recombination leading to fluorescence quenching. Moreover, DLS measurements indicated that average diameter of S,N-CDs/Fe(III) is  $358 \pm 35$  nm (Fig. S5) which is much higher than average diameter of S,N-CDs ( $47 \pm 7$  nm). This is an indication of the possibility of aggregation induced quenching between S,N-CDs and Fe(III). In addition, a minor contribution from IFE was also observed by the marginal overlapping between excitation spectrum of S,N-CDs with absorption spectrum of Fe(III) (Fig. S11). IFE is considered as an inevitable evil in quenching process associated with every fluorescence measurements due to attenuation of the excitation beam or absorption of emitted radiation by an excess concentration of S,N-CDs or by the quencher Fe(III) in solution [31]. Moreover, high ferromagnetic nature of Fe(III) may further split the discrete energy levels in S,N-CDs leading to overlap of energy levels facilitating fluorescence quenching

[15]. The possibility of this latent phenomenon has to be investigated further as it was observed that Fe(III) acts as a universal fluorescent quencher of fluorescent nanostructures, such as quantum dots, metal nanoclusters and CDs [32–34].

To investigate the selectivity of S,N-CDs towards Fe(III) over other metal cations, quenching ability of representative cations (Cu(II), Ag(I), Zn(II), Cd(II), Hg(II), Na(I), K(I), Fe(II), Co(II), Ni(II), Mg(II), Ca(II), Cr(III) and Mn(II)) were evaluated (Fig. 3d, Fig. S12). The fluorescence response was measured under the same conditions that have been studied for Fe(III). As illustrated in Fig. 3d, the maximum fluorescence quenching was obtained for Fe(III) followed by Ag(I) and Cu(II). The redox potential of Fe(III), Ag(I) and Cu(II) are positive, so these ions facilitates electron transfer induced quenching. Eventhough Hg(II) possess high redox potential, but because of the closed d orbital present in Hg(II) inhibit its electron transfer induced quenching. The selectivity of the S,N-CDs towards Fe(III) over other metal cations was attributed by, a) the high electron affinity which in turn favors electron transfer, b) paramagnetic effect of Fe(III), c) high positive reduction potential of Fe(III). Eventhough Cr(III) and Mn(II) has half filled 'd' orbital, they have negative redox potential. The quenching effect of KCl solution (Fig. 2d) did not alter the selectivity or sensitivity of S,N-CDs/Fe(III) since the investigations were carried out at high concentrations. The effect of counter anions (Cl(I), SO<sub>4</sub>(II), CH<sub>3</sub>COO(I)) on the quenching ability of Fe(III) were studied (Fig. S13) and the results showed that fluorescence intensity remain unperturbed irrespective of the anions.

### Turn on phenomenon in Fe(III) quenched S,N-CDs

Fluorescence response of Fe(III) quenched S,N-CDs towards BR was investigated by plotting  $I^1/I$ , where  $I$  is the 'Turn On' fluorescent intensity of Fe(III) quenched S,N-CDs and  $I^1$  is the fluorescent intensity of Fe(III) quenched S,N-CDs by the addition of BR. S,N-CDs is half quenched with an optimal concentration of Fe(III) 0.98 mM (S,N-CDs/Fe(III)) was employed as the fluorescent probe for further investigation. As expected, the addition of BR to the solution of S,N-CDs/Fe(III), restored its fluorescence (Fig. 4b). The plot depicting increase in fluorescence intensity of S,N-CDs/Fe(III) versus BR concentrations is linear over a concentration range of 0.2 nM to 2 nM with a limit of detection 0.12 nM (Fig. 4c). Turn on was studied over the entire concentration range from 2.18 pM to 0.21  $\mu$ M and is shown in Fig. S14. The various present methods reported for bilirubin detection is compared in Table 1. Compared to the existing methods for BR detection, present work have detection limit as low as 0.12 nM. The fluorescent enhancement in presence of BR may be due to the stronger binding affinity between BR and Fe(III). BR consists of an open chain tetra pyrrole ring structure. It has anti-oxidant property [39] which can be utilized for the detection of BR.

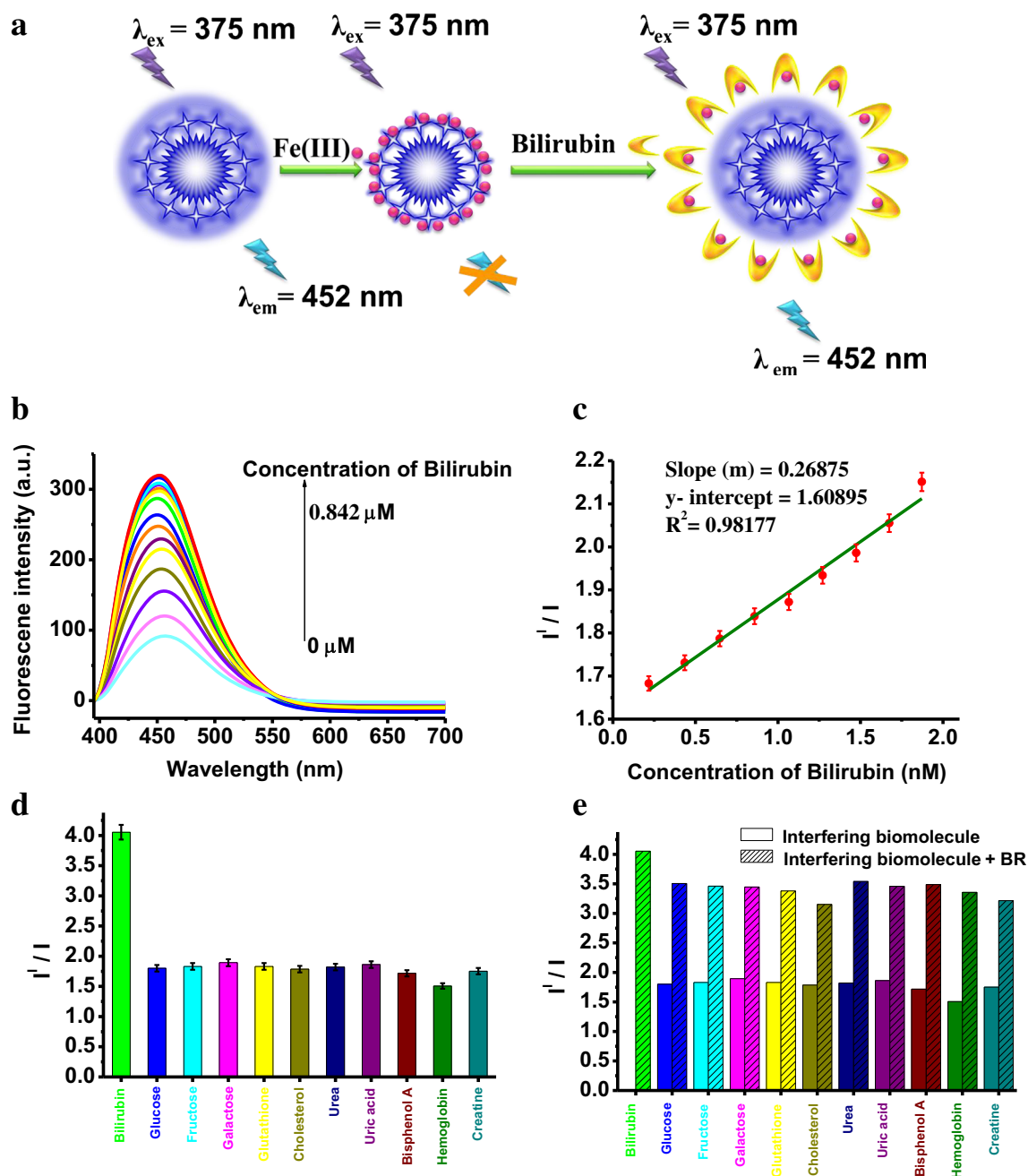


**Fig. 4** **a** Schematic illustration of Turn On phenomena in Fe(III) quenched S,N-CDs (probe) using bilirubin. **b** The fluorescence Turn On response of bilirubin towards Fe(III) quenched S,N-CDs; ([Fe(III)] = 0.98 mM; [bilirubin] = 0–0.842  $\mu$ M; pH = 2.5;  $\lambda_{\text{ex}}$  = 375 nm). **c** Linear plot revealing fluorescence enhancement of Fe(III) quenched S,N-CDs ( $I^I/I$ ) with increasing concentration of bilirubin;  $I$  and  $I^I$  are the

fluorescence intensity before and after the addition of bilirubin to S,N-CDs quenched with 0.98 mM Fe(III). ([bilirubin] = 0.2 nM–2 nM). **d** Selectivity of Fe(III) quenched S,N-CDs probe with various biomolecules; ([biomolecules] = 0.1266 nM). **e** Sensitivity studies of Fe(III) quenched S,N-CDs probe with various biomolecules; ([biomolecules] = 0.1266 nM)

When BR comes into contact with S,N-CDs/Fe(III) an electron transfer reaction may take place between the lone pair of nitrogen atoms present in the pyrrole ring of BR and Fe(III) enabling a complex formation between them. Furthermore, DLS measurements indicate that average diameter of turn on system is  $116 \pm 6$  nm. This is much lower compared to average diameter of S,N-CDs/Fe(III) ( $358 \pm 35$  nm). This

restoration in size confirms fluorescence turn on was due to the rupturing of Fe(III) mediated supramolecular aggregates of S,N-CDs. The maximum fluorescence recovery was observed at acidic pH (Fig. S15). Fluorescence lifetime of turn on system ( $7.7 \pm 0.1$  ns) is slightly higher compared to the lifetime of Fe(III) quenched S,N-CDs ( $7.6 \pm 0.4$  ns) and is in close agreement with the lifetime of S,N-CDs ( $7.8 \pm 0.2$  ns)

**Table 1** Comparison of different analytical methods for bilirubin detection

Transducer	Method	Linear range	Limit of detection	Reference
Spectrophotometry (Peroxidase method)	Bilirubin interference in uricase-peroxidase coupled reaction.	10–125 $\mu\text{M}$	Not specified	[35]
Spectrophotometry (Diazo method)	Diazotisation- 2,4 dichloroaniline diazotized and its coupling with bilirubin	85–855 $\mu\text{M}$	Not specified	[36]
Electrochemical detection (Amperometry)	Gold nanoclusters-Covalently immobilized HSA protected gold nanoclusters over indium tin oxide	0.2–7 $\mu\text{M}$	86.32 nM	[37]
Fluorimetry (turn off)	Fluorescence quenching of polyfluorene	25–50 $\mu\text{M}$	150 nM	[38]
Fluorimetry (turn off)	Gold nanoclusters-Fluorescence quenching of HSA protected gold nanoclusters	1–50 $\mu\text{M}$	248 $\pm$ 12 nM	[4]
Colorimetry	Gold nanoclusters-Peroxidase like catalytic oxidation of HSA protected gold nanoclusters	0.25–2 $\mu\text{M}$	200 $\pm$ 19 nM	[4]
Fluorimetry (turn on)	Gold nanoclusters-Fluorescence enhancement of copper ion quenched gold nanoclusters	Not specified	3.42 $\mu\text{M}$	[2]
Fluorimetry (turn on)	Fluorescence enhancement of Ferric ion quenched S,N-CDS	0.2–2 nM	0.12 nM	Present work

establishing that regeneration of the fluorescence by the formation of free S,N-CDs (Fig. S16). BR detection was also carried out in S,N-CDs quenched with Ag(I) and Cu(II) and results shows that addition of BR to such quenched system creates further quenching rather than turn on establishing the selectivity of BR towards Fe(III) quenched S,N-CDs (Fig. S17). Furthermore, time dependent nature of fluorescent turn on phenomenon by BR towards the probe was investigated. Interestingly, it was observed that after standing for 10 min in daylight, turn on was increased due to photoisomerisation of BR (Fig. S18). Upon absorbing light from the blue region of the visible spectrum, one of the C = C double bonds (adjacent to five membered ring in BR) undergoes isomerization and the configuration changes from Z,Z-BR to Z,E-BR. (Fig. S19). Z,Z form of BR is indulged in internal hydrogen bonding and hence insoluble in water. But Z,E form of BR have more polar groups exposed to the environment rendering BR water solubility and exhibits more affinity towards Fe(III) [40].

### Selectivity and sensitivity

To investigate the selectivity of BR, several co-existing biomolecules such as glucose, fructose, galactose, glutathione, creatine, cholesterol, hemoglobin (Hb), urea and uric acid were analyzed [41]. Among these, BR induces a significant increase in fluorescence intensity (Fig. 4d). Sensitivity of BR towards the probe S,N-CDs/Fe(III) with these biomolecules were carried out (Fig. 4e, Fig. S20) and showed better fluorescence recovery even in presence of interfering biomolecules.

### Real sample analysis

Performance of the probe was monitored in human urine. Urine sample of a person with clinical conditions such as chronic kidney disease (creatinine level > 5.10 mM),

hyperglycemia (glucose level > 9.15 mM) and uremic conditions (urea level > 0.15 M) may contain biomolecules in elevated concentration. So, it was necessary to compare the individual turn on response of these competing biomolecules with BR in aforementioned concentration and found out that turn on was maximum for BR (Fig. 5a). The figure depicts change in fluorescence intensities after and before BR addition ( $I^1-I$ ) on S,N-CDs/Fe(III). The cumulative effect of urea, glucose and creatine towards S,N-CDs/Fe(III) was also studied. Even in the cumulative presence of these co-existing biomolecules, BR shows significant turn on (Fig. S21). Fluorescence recovery was studied for BR spiked water as well as in urine sample at different logarithmic dilutions (Fig. 5b) and successful results were obtained. However, small turn on signals created by co-existing biomolecules such as creatine, glucose, urea and Hb causes slight concern. These small false positive signals can be considered as a blessing in disguise as clinicians can cleverly correlate these signals arising from the presence of creatine, glucose and urea in urine sample as a complimentary diagnostic tool for hyperglycemia, chronic kidney disease and uremic conditions. Slight false positive signals arising from the presence of Hb can be correlated to the possibility of other clinical conditions such as urinary tract infections, bladder cancer and judiciously ruling out the possibility of non specific periodic appearance of Hb in urine samples. Further investigations have to be conducted in future to silence the signals created by these co-existing biomolecules. Detection of BR in human serum sample was also investigated. Appropriate dilutions of the sample (10, 100 and 1000 times) were used to detect BR at two different concentrations since the level of BR in hyperbilirubinemia condition is different for newborns (340  $\mu\text{M}$ ) and in adults (170  $\mu\text{M}$ ) [2]. A quantitative recovery of the spiked BR is obtained as shown in Fig. 5c, with a recovery of 84–116%. The data indicated that this fluorescent probe has good



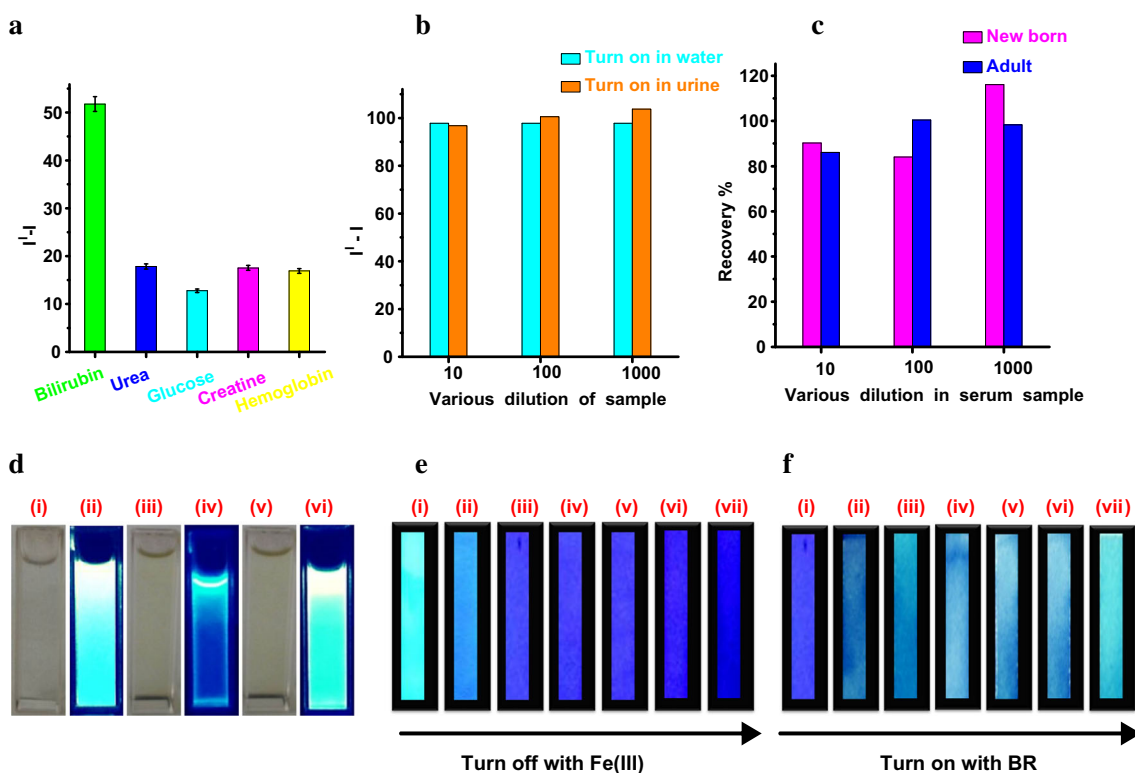


**Fig. 5** **a** Fluorescence recovery studies carried out in S,N-CDs quenched with 0.98 mM Fe(III) probe in urine sample spiked with bilirubin (0.276 μM), urea (0.1548 M), glucose (9.158 mM), creatine (5.109 mM) and hemoglobin (1 μM). **b** Change in fluorescence intensities after and before bilirubin addition on Fe(III) quenched S,N-CDs with bilirubin spiked urine sample at different dilutions (10, 100, 1000 times). ([bilirubin] = 0.276 μM). **c** Recovery percentage of bilirubin spiked serum sample at various dilutions (10, 100, 1000 times) ([bilirubin] of new born in hyperbilirubinemia condition = 340 μM (pink), [bilirubin] of adult in hyperbilirubinemia condition = 170 μM (blue)). **d** Photograph of cuvette containing (i) S,N-CDs under daylight, (ii) S,N-CDs under UV illumination (366 nm) (iii) S,N-CDs quenched

with Fe(III) under daylight (iv) S,N-CDs quenched with Fe(III) under UV illumination (v) S,N-CDs quenched with Fe(III) and turned on with bilirubin under daylight (vi) S,N-CDs quenched with Fe(III) and turned on with BR under UV illumination. **e** Photograph under UV illumination (@ 366 nm) of filter paper strip impregnated with S,N-CDs and quenched with varying concentration of Fe(III) (i) 0 mM, (ii) 1 mM, (iii) 5 mM, (iv) 10 mM, (v) 15 mM, (vi) 20 mM, (vii) 25 mM. **f** Photograph under UV illumination (@ 366 nm) of filter paper strip impregnated with S,N-CDs & soaked in 5 mM Fe(III) then dried and later turned on with varying concentration of bilirubin (i) 0 μM (ii) 0.332 μM (iii) 0.665 μM (iv) 0.998 μM (v) 1.331 μM (vi) 1.664 μM (vii) 1.996 μM

selectivity towards BR. Fig. 5d shows fluorescence of S,N-CDs, S,N-CDs/Fe(III), S,N-CDs/Fe(III)/BR under day light and UV light.

### Paper-stripe based detection

For practical application, a paper based test stripe has been designed. Whatmann no.40 filter paper was soaked in a solution containing S,N-CDs for 24 h and then dried. Under UV illumination (366 nm), the paper stripe shows blue emission. This paper stripe further soaked and dried in a solution containing 5 mM Fe(III) and the quenching of fluorescence was observed under UV illumination. The resulted filter paper was used as the probe for the detection of BR (Fig. 5e-f). Fluorescence turn on increases with increasing concentration of BR, and can be easily visualized under UV illumination (366 nm). These observations made it clear that paper based test stripe can be successfully used for the visual detection of BR.

### Conclusion

In summary, we have demonstrated a turn on fluorescence assay for the detection of bilirubin using blue fluorescent S,N-CDs. The S,N-CDs was then characterized using HRTEM, DLS, ATR-FTIR, UV-Vis and TCSPC lifetime instruments. The fluorescence was quenched with ferric ion via a static quenching mechanism and was then restored by the addition of bilirubin with limit of detection in nanomolar range. Real sample assay faced slight individual interferences from coexisting biomolecules which was observed to be nullified by the cumulative presence of biomolecules. Furthermore, bilirubin detection was investigated in biological fluids such as serum and urine and showed good recovery percentage. The current work was utilized to develop paper based test stripe for detection of bilirubin. The insight gained from these results can be utilized for the future development of point of care diagnostic devices.

**Acknowledgements** The authors acknowledge the Professor and Head of the Department of Chemistry, University of Kerala for providing the research facilities. Authors also appreciate SAIF, MGU – India.

**Compliance with ethical standards** The author(s) declare that they have no competing interests.

## References

- Tikmani SS, Warraich HJ, Abbasi F, Rizvi A, Darmstadt GL, Zaidi AK (2010) Incidence of neonatal hyperbilirubinemia: a population-based prospective study in Pakistan. *Tropical Med Int Health TM & IH* 15(5):502–507. <https://doi.org/10.1111/j.1365-3156.2010.02496.x>
- Basu S, Sahoo AK, Paul A, Chattopadhyay A (2016) Thumb imprint based detection of hyperbilirubinemia using luminescent gold nanoclusters. *Sci Rep* 6:39005. <https://doi.org/10.1038/srep39005> <https://www.nature.com/articles/srep39005#supplementary-information>
- Maisels MJ (2015) Managing the jaundiced newborn: a persistent challenge. *CMAJ* 187(5):335–343. <https://doi.org/10.1503/cmaj.122117>
- Santhosh M, Chinnadaya SR, Kakoti A, Goswami P (2014) Selective and sensitive detection of free bilirubin in blood serum using human serum albumin stabilized gold nanoclusters as fluorometric and colorimetric probe. *Biosens Bioelectron* 59:370–376. <https://doi.org/10.1016/j.bios.2014.04.003>
- Zhang JJ, Cheng FF, Li JJ, Zhu J-J, Lu Y (2016) Fluorescent nanoprobe for sensing and imaging of metal ions: recent advances and future perspectives. *NanoToday* 11:309–329. <https://doi.org/10.1016/j.nantod.2016.05.010>
- Li JJ, Cheng FF, Huang H, Li L, Li J-J (2015) Nanomaterial based activatable imaging probes: from design to biological applications. *Chem Soc Rev* 44:7855. <https://doi.org/10.1039/c4cs00476k>
- Xu Q, Kuang T, Liu Y, Cai L, Peng X, Sreenivasan Sreepasad T, Zhao P, Yu Z, Li N (2016) Heteroatom-doped carbon dots: synthesis, characterization, properties, photoluminescence mechanism and biological applications. *J Mater Chem B* 4(45):7204–7219. <https://doi.org/10.1039/C6TB02131J>
- Lim SY, Shen W, Gao Z (2015) Carbon quantum dots and their applications. *Chem Soc Rev* 44(1):362–381. <https://doi.org/10.1039/C4CS00269E>
- Miao X, Yan X, Dan Q, Li D, Tao FF, Sun Z (2017) Red emissive sulfur, nitrogen doped carbon dots and their application in ion detection and theranostics. *ACS Appl Mater Interfaces* 9:18549–18556. <https://doi.org/10.1021/acsami.7b04514>
- Zohu X, Gao X, Liu M, Wang C, Chu F (2017) A poly (5-Indolylboronic acid) based molecular imprint doped with carbon dots for fluorometric determination of glucose. *Microchim Acta* 184:4175–4181. <https://doi.org/10.1007/s00604-017-2448-0>
- Wang R, Wang X, Sun Y (2017) Aminophenol-based carbon dots with dual wavelength fluorescence emission for determination of heparin. *Microchim Acta* 184(1):187–193. <https://doi.org/10.1007/s00604-016-2009-y>
- Yang H, Li F, Zou C, Huang Q, Chen D (2017) Sulfur-doped carbon quantum dots and derived 3D carbon nanoflowers are effective visible to near infrared fluorescent probes for hydrogen peroxide. *Microchim Acta* 184(7):2055–2062. <https://doi.org/10.1007/s00604-017-2181-8>
- Dong Y, Wang R, Tian W, Chi Y, Chen G (2014) “Turn-on” fluorescent detection of cyanide based on polyamine functionalized carbon quantum dots. *RSC Adv* 4:3701. <https://doi.org/10.1039/c3ra45893h>
- Dai H, Shi Y, Wang Y, Sun Y, Hu J, Ni P, Li Z (2014) A carbon dot based biosensor for melamine detection by fluorescence resonance energy transfer. *Sensors Actuators B Chem* 202:201–208. <https://doi.org/10.1016/j.snb.2014.05.058>
- Anjali Devi JS, Salini S, Anulekshmi AH, Praveen GL, Sony G (2017) Fe (III) ion modulated I-DOPA protected gold nanocluster probe for fluorescence turn on sensing of ascorbic acid. *Sensors Sens Actuators B Chem* 246:943–951. <https://doi.org/10.1016/j.snb.2017.02.151>
- Dhenadhayalan N, Lin K-C, Suresh R, Ramamurthy P (2016) Unravelling the multiple emissive states in citric-acid-derived carbon dots. *J Phys Chem C* 120(2):1252–1261. <https://doi.org/10.1021/acs.jpcc.5b08516>
- Pan L, Sun S, Zhang A, Jiang K, Zhang L, Dong C, Huang Q, Wu A, Lin H (2015) Truly fluorescent excitation-dependent carbon dots and their applications in multicolor cellular imaging and multidimensional sensing. *Adv Mater (Deerfield Beach, Fla)* 27(47):7782–7787. <https://doi.org/10.1002/adma.201503821>
- Margraf JT, Strauss V, Guldi DM, Clark T (2015) The electronic structure of amorphous carbon nanodots. *J Phys Chem B* 119(24):7258–7265. <https://doi.org/10.1021/jp510620j>
- Yin J, Ren W, Yang G, Duan J, Huang X, Fang R, Li C, Li T, Yin Y, Hou Y, Kim SW, Wu G (2016) L-cysteine metabolism and its nutritional implications. *Mol Nutr Food Res* 60(1):134–146. <https://doi.org/10.1002/mnfr.201500031>
- Chen Y, Wu Y, Weng B, Wang B, Li C (2016) Facile synthesis of nitrogen and sulfur co-doped carbon dots and application for Fe(III) ions detection and cell imaging. *Sensors Actuators B Chem* 223:689–696. <https://doi.org/10.1016/j.snb.2015.09.081>
- Amjadi M, Manzoori JL, Hallaj T, Azizi N (2017) Sulfur and nitrogen co-doped carbon quantum dots as the chemiluminescence probe for detection of Cu<sup>2+</sup> ions. *J Lumin* 182:246–251. <https://doi.org/10.1016/j.jlumin.2016.10.021>
- Schneider J, Reckmeier CJ, Xiong Y, von Seckendorff M, Susa AS, Kasák P, Rogach AL (2017) Molecular fluorescence in citric acid-based carbon dots. *J Phys Chem C* 121(3):2014–2022. <https://doi.org/10.1021/acs.jpcc.6b12519>
- Liu Y, Zhou L, Li Y, Deng R, Zhang H (2017) Highly fluorescent nitrogen-doped carbon dots with excellent thermal and photo stability applied as invisible ink for loading important information and anti-counterfeiting. *Nano* 9(2):491–496. <https://doi.org/10.1039/C6NR07123F>
- Zhang Y, He J (2015) Facile synthesis of S, N co-doped carbon dots and investigation of their photoluminescence properties. *Phys Chem Chem Phys* 17(31):20154–20159. <https://doi.org/10.1039/C5CP03498A>
- Ding H, S-B Y, Wei J-S, Xiong H-M (2016) Full-color light-emitting carbon dots with a surface-state-controlled luminescence mechanism. *ACS Nano* 10(1):484–491. <https://doi.org/10.1021/acsnano.5b05406>
- Hong G, Diao S, Antaris AL, Dai H (2015) Carbon Nanomaterials for biological imaging and nanomedicinal therapy. *Chem Rev* 115(19):10816–10906. <https://doi.org/10.1021/acs.chemrev.5b00008>
- Park Y, Yoo J, Lim B, Kwon W, Rhee SW (2016) Improving the functionality of carbon nanodots: doping and surface functionalization. *J Mater Chem A* 4(30):11582–11603. <https://doi.org/10.1039/C6TA04813G>
- Dutta Choudhury S, Chethodil JM, Gharat PM, Praseetha PK, Pal H (2017) pH-elicited luminescence functionalities of carbon dots: mechanistic insights. *J Phys Chem Lett* 8(7):1389–1395. <https://doi.org/10.1021/acs.jpcclett.7b00153>
- Zu F, Yan F, Bai Z, Xu J, Wang Y, Huang Y, Zhou X (2017) The quenching of the fluorescence of carbon dots: a review on mechanisms and applications. *Microchim Acta* 184(7):1899–1914. <https://doi.org/10.1007/s00604-017-2318-9>
- Yoosaf K, Ipe BL, Suresh CH, Thomas KG (2007) In situ synthesis of metal nanoparticles and selective naked-eye detection of lead ions from aqueous media. *J Phys Chem C* 111(34):12839–12847. <https://doi.org/10.1021/jp073923q>

31. Li G, Fu H, Chen X, Gong P, Chen G, Xia L, Wang H, You J, Wu Y (2016) Facile and sensitive fluorescence sensing of alkaline phosphatase activity with Photoluminescent carbon dots based on inner filter effect. *Anal Chem* 88(5):2720–2726. <https://doi.org/10.1021/acs.analchem.5b04193>
32. Li S, Li Y, Cao J, Zhu J, Fan L, Li X (2014) Sulfur-doped graphene quantum dots as a novel fluorescent probe for highly selective and sensitive detection of Fe<sup>3+</sup>. *Anal Chem* 86(20):10201–10207. <https://doi.org/10.1021/ac503183y>
33. Tang T, Ouyang J, Hu L, Guo L, Yang M, Chen X (2016) Synthesis of peptide templated copper nanoclusters for fluorometric determination of Fe(III) in human serum. *Microchim Acta* 183(10):2831–2836. <https://doi.org/10.1007/s00604-016-1935-z>
34. Li G, Lv N, Bi W, Zhang J, Ni J (2016) Nitrogen-doped carbon dots as a fluorescence probe suitable for sensing Fe<sup>3+</sup> under acidic conditions. *New J Chem* 40(12):10213–10218. <https://doi.org/10.1039/C6NJ02088G>
35. Hullin DA, McGrane MT (1991) Effect of bilirubin on uricase-peroxidase coupled reactions. Implications for urate measurement in clinical samples and external quality assessment schemes. *Ann Clin Biochem* 28(Pt 1):98–100. <https://doi.org/10.1177/000456329102800117>
36. Rand RN, Ad P (1962) A new Diazo method for the determination of bilirubin. *Clin Chem* 8(6):570–578
37. Santhosh M, Chinnadayala SR, Singh NK, Goswami P (2016) Human serum albumin-stabilized gold nanoclusters act as an electron transfer bridge supporting specific electrocatalysis of bilirubin useful for biosensing applications. *Bioelectrochemistry (Amsterdam, Netherlands)* 111:7–14. <https://doi.org/10.1016/j.bioelechem.2016.04.003>
38. Senthilkumar T, Asha SK (2015) Selective and sensitive sensing of free bilirubin in human serum using water-soluble Polyfluorene as fluorescent probe. *Macromolecules* 48(11):3449–3461. <https://doi.org/10.1021/acs.macromol.5b00043>
39. Jansen T, Daiber A (2012) Direct antioxidant properties of bilirubin and Biliverdin. Is there a role for biliverdin reductase? *Front Pharmacol* 3:30. <https://doi.org/10.3389/fphar.2012.00030>
40. Fevery J (2008) Bilirubin in clinical practice: a review. *Liver Int* 28(5):592–605. <https://doi.org/10.1111/j.1478-3231.2008.01716.x>
41. Wu H, Jiang J, Gu X, Tong C (2017) Nitrogen and sulfur co-doped carbon quantum dots for highly selective and sensitive fluorescent detection of Fe(III) ions and L-cysteine. *Microchim Acta* 184(7):2291–2298. <https://doi.org/10.1007/s00604-017-2201-8>